Electrochimica Acta 296 (2019) 945–953

Contents lists available at ScienceDirect

Electrochimica Acta

journal homepage: www.elsevier.com/locate/electacta

Polymer-assisted approach to $LaCo_{1-x}Ni_xO_3$ network nanostructures as bifunctional oxygen electrocatalysts

Haizhen Wang, Weichuan Xu, Stephanie Richins, Kevin Liaw, Litao Yan, Meng Zhou, Hongmei Luo*

Department of Chemical and Materials Engineering, New Mexico State University, Las Cruces, NM, 88003, United States

ARTICLE INFO

Article history:
Received 4 September 2018
Received in revised form
6 November 2018
Accepted 11 November 2018
Available online 21 November 2018

Keywords:
Polymer-assisted
Perovskites
Network structures
OER and ORR
Bifunctionality

ABSTRACT

Energy depletion caused by the consumption of fossil fuels due to increasing population and economic growth has stimulated intense research on electrochemical energy storage systems, including fuel cells and metal-air batteries. Oxygen electrocatalysis, including both oxygen reduction reaction (ORR) and oxygen evolution reaction (OER), dominates the performance of these electrochemical energy systems. However, the sluggish kinetics of these two reactions still limits their performance and even the commercialization of these electrochemical energy storage systems. Therefore, development of non-precious metal-based oxygen catalysts, especially with bifunctionality for both OER and ORR, is greatly demanded. In this report, polymer-assisted approach has been employed to synthesize $LaCoO_3$-based perovskite nanoparticles, which interconnected together to form porous network structures. X-ray diffraction indicated that replacement of Co with Ni would lead to a lattice expansion due to larger ionic radius of Ni^{3+} as compared to that of Co^{3+}. The electrocatalytic activity of these materials in 0.1 M KOH aqueous solution showed that ORR performance of $LaCoO_3$ can be improved through incorporation of Ni into the B-site while their OER performance will also be enhanced which renders these perovskite oxides to exhibit better bifunctional electrocatalytic activity for both OER and ORR. The enhanced performance with Ni-doping might be due to the synergistic effect from the two transition metals as a result of the formation of new redox couples Ni^{3+}/Ni^{2+} as well as the higher Co^{3+}/Co^{2+} ratio, which could promote adsorption of oxygen on the catalytic surface with improved the Co–O bond strength. Our study not only introduces polymer-assisted method to prepare network structured perovskite nanoparticles, but also highlights the importance of B-site metal doping in perovskites as a simple strategy to enhance their bifunctional oxygen catalytic activities.

1. Introduction

The consumption of fossil fuels due to population growth and economic development has expedited the energy depletion and various environmental issues, which stimulated worldwide research on new energy conversion and storage systems that are highly efficient, environmentally friendly with low lost, such as fuel cells [1,2] and metal-air batteries [3]. Oxygen reduction reaction (ORR) in alkaline media acts as the cathode reaction in those electrochemical energy converting devices while oxygen evolution reaction (OER) is the anodic reaction in regenerative fuel cells and takes place during the charging process of the lithium-air batteries [4], which requires large potentials, thus higher energy input. Therefore, efficient ORR and OER are of great importance in these energy storage systems since they govern the performance of these electrochemical energy systems. Due to the sluggish kinetics in OER and ORR, various catalysts have been investigated in order to reduce the overpotential for these two reactions. Up to now, platinum-based materials [1,5] are known to be the most active catalysts for ORR but only haves moderate activity for OER while Ruthenium (Ru) [6] and Iridium oxides (IrO_2) [7] show superior catalytic performance for OER than ORR. Besides, the scarcity [8] and high cost [9] of these noble metal catalysts as well as the declining activity during operation still limits their practical applications on a large scale and even the commercialization of fuel cells and metal-air batteries. Therefore, alternative efficient catalysts based on non-precious metal/metal composites, especially

* Corresponding author.
E-mail address: hluo@nmsu.edu (H. Luo).

https://doi.org/10.1016/j.electacta.2018.11.075
0013-4686/

bifunctional catalysts which are active towards both ORR and OER, are highly demanded.

Up to date, a variety of materials, including non-precious metal oxides [8,10–12], and graphene-based materials [4], have been investigated and showed potential applications as bifunctional catalysts for both ORR and OER. Among them, perovskite oxides [12–16], a new class in the family of mixed transition metal oxides, have emerged as new catalyst candidates due to their structural, thermal and chemical stability. The general formula of perovskite oxides is ABO_3, where A is a typical lanthanide, alkaline or alkaline-earth cation and B is transition metal cation, such as Mn, Co, Fe and Ti [17]. They consist of corner-shaped BO_6 octahedra together with A-site cations at the corner of the unit cell. Besides, perovskite oxides with low price and good endurance under relatively high temperature can be doped with a wide range of cations on A-site and/or B-site due to the flexibility of their compositions and structures, which allows easy manipulation of their catalytic properties, including bifunctional electrocatalytic activities in both OER and ORR. The application of perovskite metal oxides as oxygen catalysts has been first reported in the early 1970s [18]. Since then, perovskite oxides, especially La-based [8,11], as bifunctional catalysts for both ORR and OER have attracted increasingly attention and become one of the hottest topics in the field of electrocatalysis. Several approaches have been proposed to increase the catalytic activities of perovskites, including A-site deficiency creation [8,9,11] to introduce oxygen vacancy and tune the electronic structure, B-site metal doping [15,19] to provide more redox active sites and particle size/morphology engineering [20,21] to increase the surface area of the catalysts.

In terms of the perovskite oxide preparation, several approaches have been developed to obtain metal oxides with different morphologies and particle sizes, including hydrothermal/solvothermal method [16,22], combustion synthesis [23,24], co-precipitation [25] and sol-gel [26] method, etc. For $LaCo_{1-x}Ni_xO_3$ materials, both the conventional solid state method [27–29] or citric acid-assisted Pechini method [30,31] have been utilized. However, either complicated procedures involved in these methods (either using high reaction temperature or extra equipment such as freeze-dryer) or the large particle size of perovskites obtained, limits their practical applications. In order to get perovskite with smaller particle size and comparatively higher surface area, a facile polymer-assisted method has been developed [8] and proposed to synthesize perovskite metal oxides [11,32]. Polymer-assisted deposition, an aqueous solution approach, was first introduced in 2004 [33] for uniform film growth. In this method, two polymers, including ethylenediaminetetraacetic acid (EDTA) and polyethyleneimine (PEI), are used to combine with metal ions to form metal-polymer complexes [32,34], in which the viscosity of the solutions can be controlled by tuning the amount of polymer added and thereby the particle growth. A variety of metal oxides can be synthesized via this method since polymers could combine with almost any metal ions by electrostatic attraction, hydrogen bonding or covalent bonding and nanoparticles with comparatively smaller particle size could be achieved.

Cobalt-based materials are promising candidates for bifunctional oxygen catalysts [35] due to their good performance in both OER and ORR, as well as their potential for improvement with different synthetic routes. Compared with other perovskite oxides, $LaCoO_3$ has been observed to exhibit better electrocatalytic activity [21]. In order to further enhance its bifunctionality for OER and ORR, B-site doping with nickel has been employed in this paper since the combination of two different ions at B-site induces synergistic effects [15] for the catalyst design, leading to better catalytic performance. $LaCo_{1-x}Ni_xO_3$ nanostructures have been demonstrated as electrocatalyst for water oxidation and zinc-air battery before [36]. However, the electrospinning method they used needs electrospinning instrument as well as very tedious work. In this paper, we have utilized polymer-assisted method to prepare $LaCo_{1-x}Ni_xO_3$ nanomaterials. First, $LaCoO_3$ nanoparticles have been synthesized using the polymer-assisted approach and nickel was then introduced into the B-site of $LaCoO_3$. The electrocatalytic performance of the as-prepared Ni-incorporated perovskites for both OER and ORR has been investigated, which showed that the ORR performance of $LaCo_{1-x}Ni_xO_3$ can be enhanced with the inclusion of Ni, while the OER also displayed increased performance, resulting in the improvement of the bifunctionality of the perovskite metal oxides as oxygen catalysts. This study not only introduces polymer-assisted method to prepare network structured perovskite oxide nanoparticles, but also highlights the importance of B-site metal doping in perovskites as a simple strategy to enhance their oxygen catalytic bifunctionality.

2. Experimental section

2.1. Materials

Poly(ethylenimine) (PEI) (50% w/v in H_2O), ethylenediaminetetraacetic acid (EDTA) (>99.4%), lanthanum nitrate ($La(NO_3)_3 \cdot 6H_2O$, 99.99%), cobalt nitrate hexahydrate ($Co(NO_3)_2 \cdot 6H_2O$), nickel nitrate hexahydrate ($Ni(NO_3)_2 \cdot 6H_2O$) and potassium hydroxide (KOH) were purchased from Sigma-Aldrich. All chemicals were used as received without further treatment.

2.2. Synthesis of $LaCoO_3$ (LCO)

2 g poly(ethylenimine) (PEI) and 1 g ethylenediaminetetraacetic acid (EDTA) were added into 10 mL deionized water in a beaker, which is sonicated until dissolved. Then 1 mmol $La(NO_3)_3 \cdot 6H_2O$ and 1 mmol $Co(NO_3)_2 \cdot 6H_2O$ were added to the previous solution, which was stirred for another few hours. Then the resultant solution was transferred to a crucible which was heated to 700 °C with a ramp rate of 1 °C/min and kept in 700 °C for 3 h.

2.3. Synthesis of $LaCo_{1-x}Ni_xO_3$ ($x = 0.1, 0.3, 0.5$)

The procedure for synthesis of $LaCo_{1-x}Ni_xO_3$ is the same as $LaCoO_3$ except that $x = 0.1, 0.3, 0.5$ mmol $Ni(NO_3)_2 \cdot 6H_2O$ was added to the solution respectively while the amount of $Co(NO_3)_2 \cdot 6H_2O$ added to the solution is correspondingly to be $1\text{-}x = 0.9, 0.7, 0.5$ mmol. The other reaction conditions would be the same as before. The four samples $LaCoO_3$, $LaCo_{0.9}Ni_{0.1}O_3$, $LaCo_{0.7}Ni_{0.3}O_3$ and $LaCo_{0.5}Ni_{0.5}O_3$ are denoted as LCO, LC9N1, LC7N3 and LC5N5, respectively.

2.4. Characterization

The structure, composition, and morphology of the samples were characterized using X-ray diffraction (XRD) and transmission electron microscopy (TEM). XRD was carried out using a PANalytical Empyrean powder diffractometer with Cu Ka ($\lambda = 1.5406$ Å) at 45 kV and 40 mA. The morphology and particle size of the samples was analyzed with transmission electron microscopy (TEM) on H-7650, Hitachi High-Technologies Corp, operating at 80 kV. The surface chemistry was studied using X-ray photoelectron spectroscopy (XPS) on a Thermo K-Alpha spectrometer equipped with a monochromatic Al kα X-ray source. The surface areas of the samples were examined by the Brunauer-Emmett-Teller (BET) with a Micromeritics ASAP 2050 instrument using the standard N_2 adsorption and desorption isotherm measurement at 77 K.

2.5. Electrochemical measurements

The electrochemical measurements were carried out using a rotating disk connected to electrochemical workstation (CHI 760C) with a potentiostat in a standard three-electrode electrochemical cell at room temperature. A Platinum (Pt) coil and Ag(s)|AgCl(s)|Cl^-(aq) (3.5 mol L^{-1} KCl) electrode were used as counter and reference electrode, respectively. The electrolyte used in the electrochemical measurements was 0.1 M KOH solution. The reference electrode was brought into contact with the cell solution through a Luggin capillary (KCl agar–agar salt bridge). Catalyst ink was prepared by dispersing 5 mg oxide powder in 1 mL H_2O with 0.05 wt % diluted Nafion®117 solution. Different from many other works, no conductive carbon was added to eliminate the resistivity limitation. After sonication, an aliquot of 10 μL catalyst ink was loaded onto a rotating disk electrode (RDE) with a 5.0 mm diameter glassy carbon. Polarization curves for the oxygen reduction reaction (at different rotation speeds of 100, 400, 900, and 1600 rpm) and oxygen evolution reaction (at a rotation speed of 1600 rpm) were tested in the electrolyte using a CHI electrochemical instrument at a scan speed of 10 mV/s. The potential values were calculated by the following equation after the iR-correction: $E_{iRcorrected} = E - iR$, where i is the measured current density and R the ohmic resistance of electrolyte solution (~49 Ω), which was measured by AC Impedance in 0.1 M KOH aqueous solution. The resistance for the perovskite oxide catalysts was characterized by electrochemical impedance spectra (EIS) at 0.7 V vs Ag(s)|AgCl(s)|Cl^-(aq) (3.5 mol L^{-1} KCl) with frequencies ranging from 100 kHz to 0.1 Hz under an AC voltage of 5 mV.

To understand the reaction mechanisms for ORR, the kinetic parameters, including the electron transfer number and the kinetic current density in ORR can be determined from the following Koutecky–Levich (K-L) equation:

$$\frac{1}{J} = \frac{1}{J_k} + \frac{1}{J_L} = \frac{1}{nFkC^0} + \frac{1}{0.62nFD_{O_2}^{2/3}\nu^{-1/6}C^0\omega^{1/2}}$$

where J corresponds to the measured current density, J_k and J_L are the kinetic and diffusion-limiting current densities, respectively, n is the electron transfer number, F is the Faraday constant (96500 C/mol), C^0 is the saturated concentration of oxygen in 0.1 M KOH, ω is the rotating rate (rad/s), D_{O2} is the diffusion coefficient of oxygen (1.73×10^{-5} cm^2/s) [16], ν is the kinetic viscosity of the solution (0.01 cm^2/s) and k is the rate constant for oxygen reduction.

3. Results and discussion

The crystal structure of the as-synthesized perovskite oxides $LaCo_{1-x}Ni_xO_3$ (x = 0, 0.1, 0.3, 0.5) was characterized by x-ray diffraction (XRD), as shown in Fig. 1. All the diffraction peaks of the samples could be assigned to rhombohedral phase with a space group of R3C which are well in agreement with the standard JCPDS card No. 54-0834. No extra peaks emerged from any of the perovskite oxides, suggesting that there were no impurities in the as-prepared samples. It was observed that the peak located in the region of 2θ at 47° in the right magnified figure shifted to lower angles with an increase of the nickel substitution. As shown in the crystal structure of $LaCo_{1-x}Ni_xO_3$ in Fig. 1b, replacement of Co with Ni would lead to a lattice expansion due to the larger ionic radius of Ni^{3+} as compared to that of Co^{3+}, resulting in the XRD peak shift to lower angles, which is consistent with the previous reports [31]. To avoid complications, the content of nickel doping was limited to 50% in our study since the topic of this report is focused on the influence of Ni doping into $LaCoO_3$ on their electrocatalytic performance.

Fig. 2 shows the morphology of the as-prepared $LaCo_{1-x}Ni_xO_3$ (x = 0, 0.1, 0.3, 0.5) samples revealed using transmission electron microscopy (TEM). It can be clearly seen that small nanoparticles interconnect together to form a porous two-dimensional network structure, which can be furthered confirmed by Fig. S1. It is also noted that the particle size of the samples decreases from around 60-100 nm (Fig. 2a) for $LaCoO_3$ to 30-80 nm (Fig. 2d) for $LaCo_{0.5}Ni_{0.5}O_3$. Accordingly, the surface area of the particles increases as estimated by N_2 adsorption-desorption isotherms and calculated based on the Brunauer-Emmett-Teller (BET) method (Fig. S2). The BET specific surface area of $LaCo_{0.5}Ni_{0.5}O_3$ is 7.45 m^2/g, larger than perovskite oxides prepared by sol-gel method (2.78 m^2/g) [14], which is due to the implementation of the polymer-assisted method. It is expected that smaller particle size with larger surface area may benefit the electrocatalytic performance of the catalysts due to the exposure of more active sites to the reactants.

X-ray photoelectron spectroscopy (XPS) was also used to examine the surface elemental composition of the samples. The survey spectra (Fig. S3) for all the as-synthesized $LaCo_{1-x}Ni_xO_3$ samples confirm the presence of La, Co and Ni in these samples after the incorporation of Ni. Fig. 3 shows the XPS spectra in the Co $2p_{3/2}$ and O 1s regions. As shown in Fig. 3a–d, the peak located at around 780 eV corresponds to the binding energy of Co $2p_{3/2}$, which can be deconvoluted into two peaks with a binding energy of 779.5 and 781.8 eV, being attributed to the surface Co^{3+} and Co^{2+} species [37]. It has been reported that Ni doping could result in the creation of new active sites from the new redox couple Ni^{3+}/Ni^{2+} [38]. However, the quantification of Ni from the Ni 2p peak could not be realized due to the overlapping Ni 2p and La 3d peaks observed [39] in the same region since they have similar binding energy values. Besides, different surface oxygen species also have been identified by O 1s XPS spectra through being deconvoluted into three peaks. The characteristic peak around 529.5 eV (red peak in Fig. 3) represents the lattice oxygen or highly oxidative oxygen species. The peak around 531.2 eV (green peak in Fig. 3) is associated with chemically adsorbed oxygen species on the oxygen vacancies. The characteristic peak around 532.5 eV can represent the physically adsorbed oxygen species on the surface (H_2O) [37]. The relative content of the different cobalt and oxygen species estimated from the relative area of these fitted peaks are listed on Table S1.

In order to evaluate the catalytic activities of the $LaCo_{1-x}Ni_xO_3$ (x = 0, 0.1, 0.3, 0.5) network structures for oxygen reduction reaction (ORR), linear sweep voltammetry (LSV) in O_2 saturated 0.1 M KOH was conducted rotating disk-electrode (RDE) measurements under different rotation rates of 100 rpm, 400 rpm, 900 rpm and 1600 rpm (Fig. S4). Fig. 4a shows the typical ORR current densities of the four materials with a scan rate of 10 mV/s under a rotation rate of 1600 rpm. It can be seen from the figure that Ni-incorporated samples ($LaCo_{0.9}Ni_{0.1}O_3$, $LaCo_{0.7}Ni_{0.3}O_3$, $LaCo_{0.5}Ni_{0.5}O_3$) showed higher limiting current density and also exhibit more positive onset potential than the pristine $LaCoO_3$, indicating better ORR activity. At a potential range which is more negative than around −0.47 V vs. Ag(s)|AgCl(s)|Cl^-(aq) (3.5 mol L^{-1} KCl), the current plateau indicates the diffusion-limited region. To further understand the ORR kinetics and electrocatalytic processes on the prepared materials, we have derived the Koutecky-Levich (K-L) plots (Fig. 4b) from the LSV curves in Fig. S4. The electron transfer number (n) at −0.4 V (vs Ag(s)|AgCl(s)|Cl^-(aq) (3.5 mol L^{-1} KCl)) can be calculated from the slope of K-L plots, which is 3.37, 3.54, 3.62 and 3.84 for $LaCoO_3$, $LaCo_{0.9}Ni_{0.1}O_3$, $LaCo_{0.7}Ni_{0.3}O_3$ and $LaCo_{0.5}Ni_{0.5}O_3$, respectively, as shown in Fig. 4c. All of them are close to four electron transfer pathways for ORR, suggesting a reversible four-electron ORR reaction ($O_2+H_2O+4e^- = 4OH^-$) domination in these catalysts. Besides, the kinetic current density

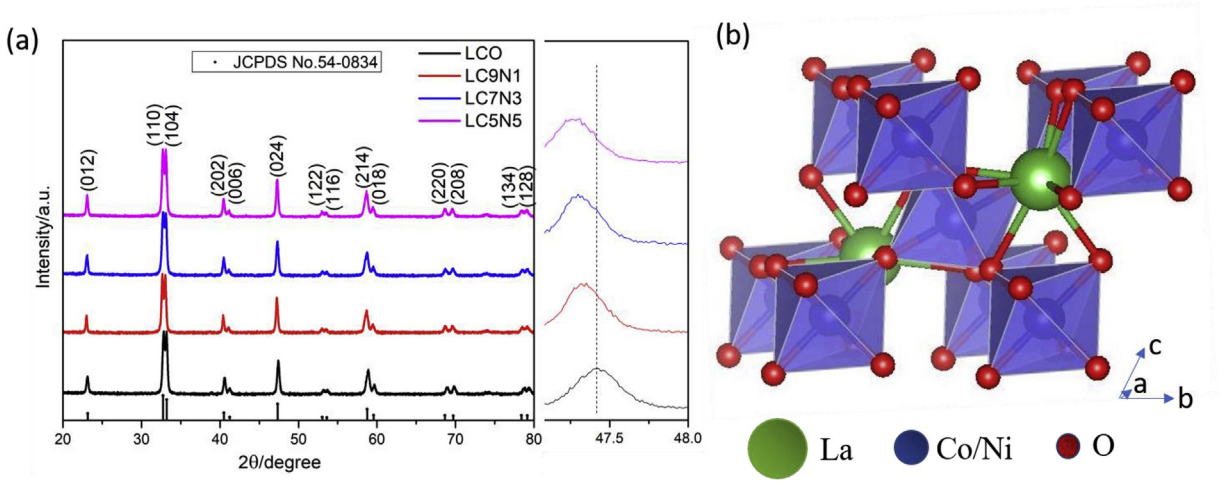

Fig. 1. (a) The XRD patterns and (b) the schematic illustration of the crystal structure of the as-synthesized $LaCo_{1-x}Ni_xO_3$ network structured materials.

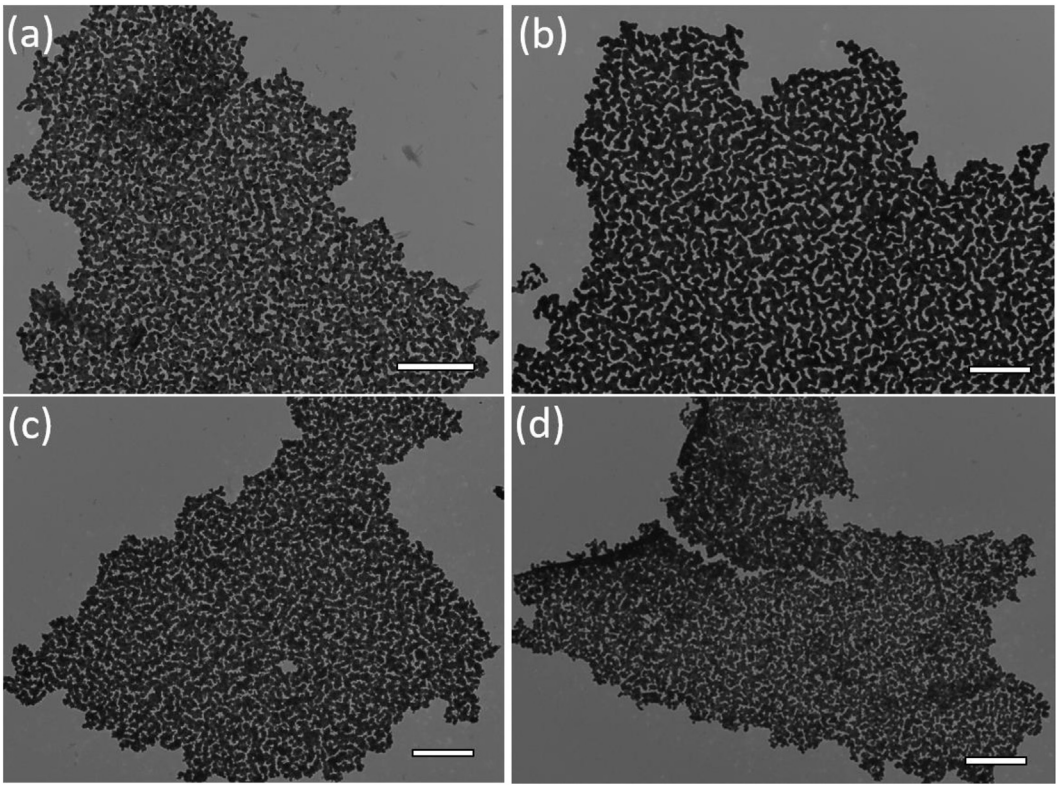

Fig. 2. TEM images of the as-prepared $LaCo_{1-x}Ni_xO_3$: (a) $LaCoO_3$, (b) $LaCo_{0.9}Ni_{0.1}O_3$, (c) $LaCo_{0.7}Ni_{0.3}O_3$, and (d) $LaCo_{0.5}Ni_{0.5}O_3$. The scale bar is 1 μm for all four figures.

values (Fig. 4c) of the catalyst at −0.4 V vs (Ag/AgCl) follow the sequence of $LaCo_{0.5}Ni_{0.5}O_3 > LaCo_{0.7}Ni_{0.3}O_3 > LaCo_{0.9}Ni_{0.1}O_3 > LaCoO_3$, which could also reflect the ORR activity of the catalysts. Tafel plots have been provided in Fig. 4d in order to gain more insights into the catalytic behavior of the catalysts. $LaCo_{0.5}Ni_{0.5}O_3$ has the smallest Tafel slope and thus has the most rapid ORR catalytic rate. The higher ORR performance of $LaCo_{0.5}Ni_{0.5}O_3$ catalyst in alkaline solution might be due to the synergistic effect from the two transition metal ions as a result of the formation of new redox couples Ni^{3+}/Ni^{2+} [35]. Besides, the higher Co^{3+}/Co^{2+} ratio (from XPS) could promote adsorption of oxygen on the catalytic surface [8] and improve the Co–O bond strength, resulting in higher ORR performance. The increased specific surface area leads to higher concentration of active sites on the catalyst surface, also resulting in the increase of the catalytic performance. However, ORR on perovskite surface is complicated. In addition to surface absorption behavior, it still depends on several factors including its intrinsic activity, electronic conductivity [40]. It is worth noting that the exact reaction mechanism of bare perovskite metal oxides $LaMO_3$ (M = metal) without conducting additives are still illusive, even for ORR catalyst Pt, there is no generally accepted mechanism [40] to date due to the elusiveness of reaction intermediates. Therefore, more fundamental study of the perovskite-based catalysts is necessary in future to understand this process clearly.

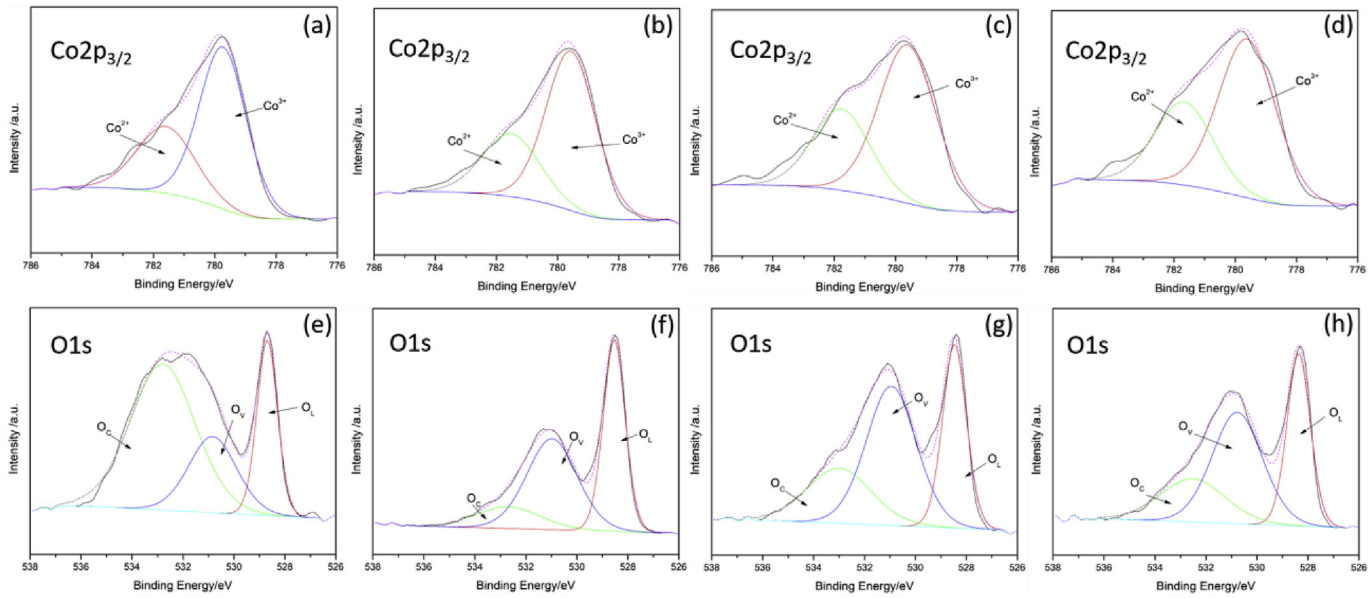

Fig. 3. Co $2p_{3/2}$ and O 1s XPS spectra and representative fitting for four different catalysts (a, e) $LaCoO_3$, (b, f) $LaCo_{0.9}Ni_{0.1}O_3$, (c, g) $LaCo_{0.7}Ni_{0.3}O_3$, and (d, h) $LaCo_{0.5}Ni_{0.5}O_3$, respectively.

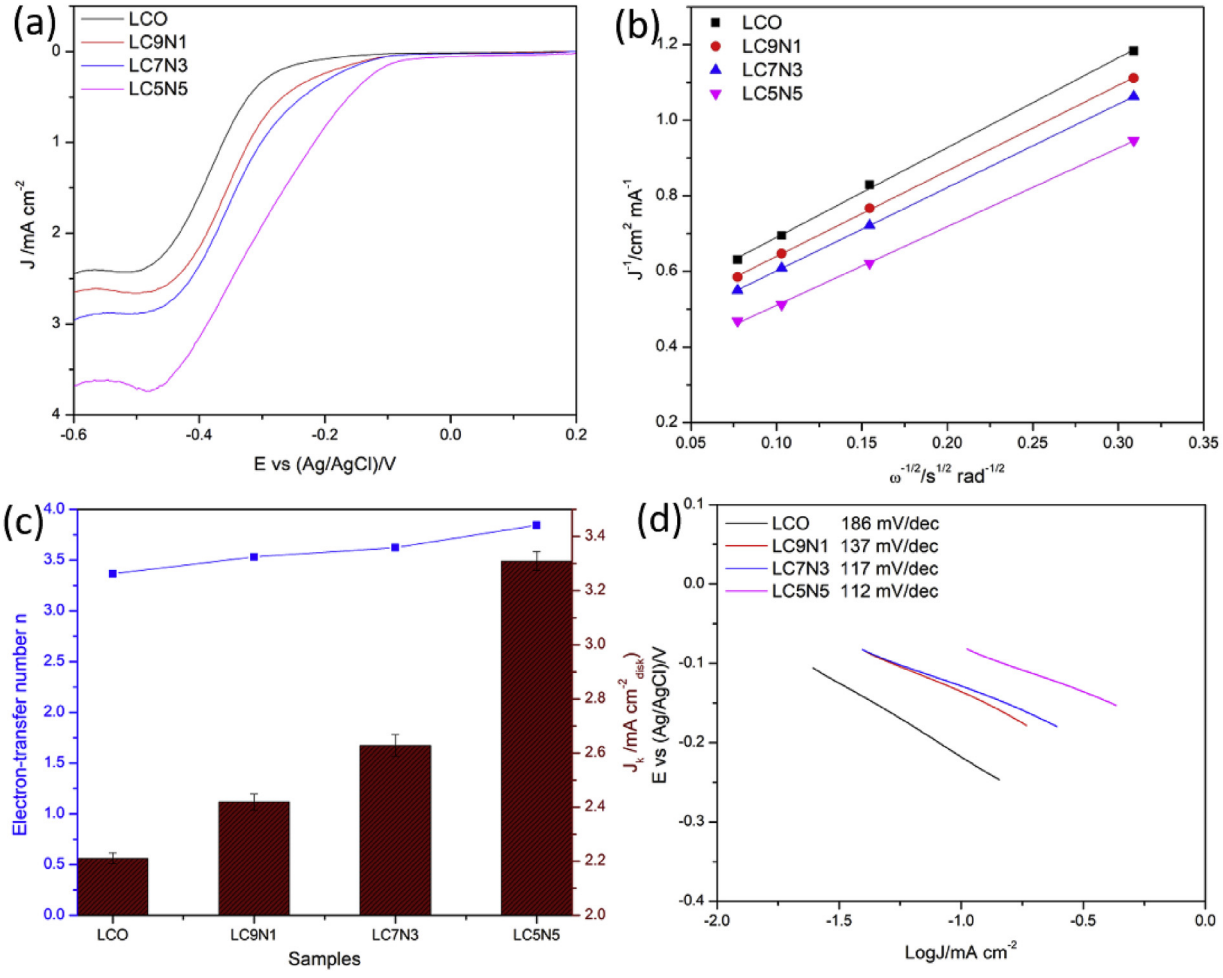

Fig. 4. (a) LSV curves for the ORR on the RDE (1600 rpm) for four samples $LaCoO_3$, $LaCo_{0.9}Ni_{0.1}O_3$, $LaCo_{0.7}Ni_{0.3}O_3$ and $LaCo_{0.5}Ni_{0.5}O_3$ in O_2 saturated 0.1 M KOH aqueous solution with a scan rate of 10 mV/s; (b) Koutecky-Levich plots of four samples at −0.4 V based on ORR polarization curves at Fig. S4; (c) the electron transfer number and the kinetic current density of the four samples at −0.4 V. The error bar is based on three repeated results; and (d) Tafel plots of OER activity for the as-prepared four samples.

To further examine whether the perovskite oxides $LaCo_{1-x}Ni_xO_3$ could be used as bi-functional catalysts, their electrocatalytic activity for OER was also evaluated by linear sweeping voltammograms (LSVs) in 0.1 M KOH electrolyte with a scan rate of 10 mV/s at a rotation speed of 1600 rpm. The LSVs in Fig. 5a clearly show that partial substitution of nickel in the octahedral site of the perovskite structure has influence on the OER activity of the samples, resulting in lower onset potential and greater catalytic current density than that of the pristine $LaCoO_3$, which implies better OER catalytic performance. The potential for achieving the current density of 10 mA/cm^2 (EJ10), a parameter to indicate the catalytic activities of the catalysts, also has been compared among these catalysts. Obviously, nickel incorporated $LaCoO_3$ ($LaCo_{0.9}Ni_{0.1}O_3$) can achieve this current density (10 mA/cm^2) at a smaller potential of around 0.65 V, which is lower than 0.68 V for pristine $LaCoO_3$. For $LaCo_{0.5}Ni_{0.5}O_3$, there is about 33 mV negative shift for the E_{J10} potential compared with $LaCoO_3$. Further normalizing the OER activity by the catalyst loading, the mass activity (Fig. 5b) of each catalyst at two different potentials has been obtained, the trend of which is consistent with the OER activities. Furthermore, Tafel plot was used to evaluate the reaction rate of OER. As shown in Fig. 5c, the $LaCo_{0.9}Ni_{0.1}O_3$ catalyst exhibits a smaller Tafel slope (64.2 mV/dec) than $LaCo_{0.7}Ni_{0.3}O_3$ (72.8 mV/dec), $LaCo_{0.5}Ni_{0.5}O_3$ (73.9 mV/dec) and $LaCoO_3$ (74.4 mV/dec), thus more rapid OER reaction rate.

The electrochemically active surface area (ECSA) of the as-synthesized electrocatalysts was examined using the electrochemical double layer capacitance by measuring the non-faradaic capacitance current associated with double layer charging at different scan rates in 0.1 M KOH electrolyte via cyclic voltammetry (CV). Fig. S5 shows the CV of the $LaCo_{1-x}Ni_xO_3$ ($x = 0, 0.1, 0.3, 0.5$) catalysts in a non-faradaic potential region. The capacitive current densities as a function of scan rate for these catalysts are given in Fig. 5d, in which the linear slope of the curves represents the double layer capacitance. However, it's difficult to figure out the exact ECSA values for multicomponent metal oxides [9]. Instead, the ECSA difference between the electrocatalysts could be compared using the double layer capacitance. As shown in Fig. 5d, the capacitance of $LaCo_{0.9}Ni_{0.1}O_3$ (0.104 mF/cm^2) is larger than the rest of the catalysts. Higher capacitance represents larger ECSA, which favors OER catalytic activity towards water splitting since larger ECSA offers more active sites to react with electrolyte for electrocatalysis [8,9]. The OER trend might also be attributed to the existence of mixed valence states of transition metals (Co^{3+}/Co^{2+} and Ni^{3+}/Ni^{2+}) with optimized composition and tunable OH-adsorption and O_2 desorption ability [38] since the various valence states determine the adsorption and desorption of hydroxide ions. Besides, with more nickel substitution, the M – O bonding will decrease, thus less hydroxyl ions (OH^-) could be absorbed onto the catalyst surface since Co–OH bond strength is higher than Ni–OH [41]. All these factors together lead to the enhancement of the OER performance of Ni-incorporated $LaCoO_3$ materials.

In order to further comprehend the kinetics of the as-prepared perovskites for OER, the electrochemical impedance spectroscopy (EIS) analysis of the $LaCo_{1-x}Ni_xO_3$ catalysts has been conducted, as shown in Fig. 5e. $LaCo_{0.9}Ni_{0.1}O_3$ has a much smaller semicircle radius than the other catalysts, indicating a much lower charge transfer resistance and thus a higher charge-transfer rate and more rapid catalytic kinetics. The equivalent circuit has been inserted in Fig. 5e, in which Rs is the uncompensated solution resistance, Rct is the charge transfer resistance, and Cdl is the constant-phase element. Rct is a critical factor in the evaluation of the electrochemical performance of the catalysts [9]. According to the

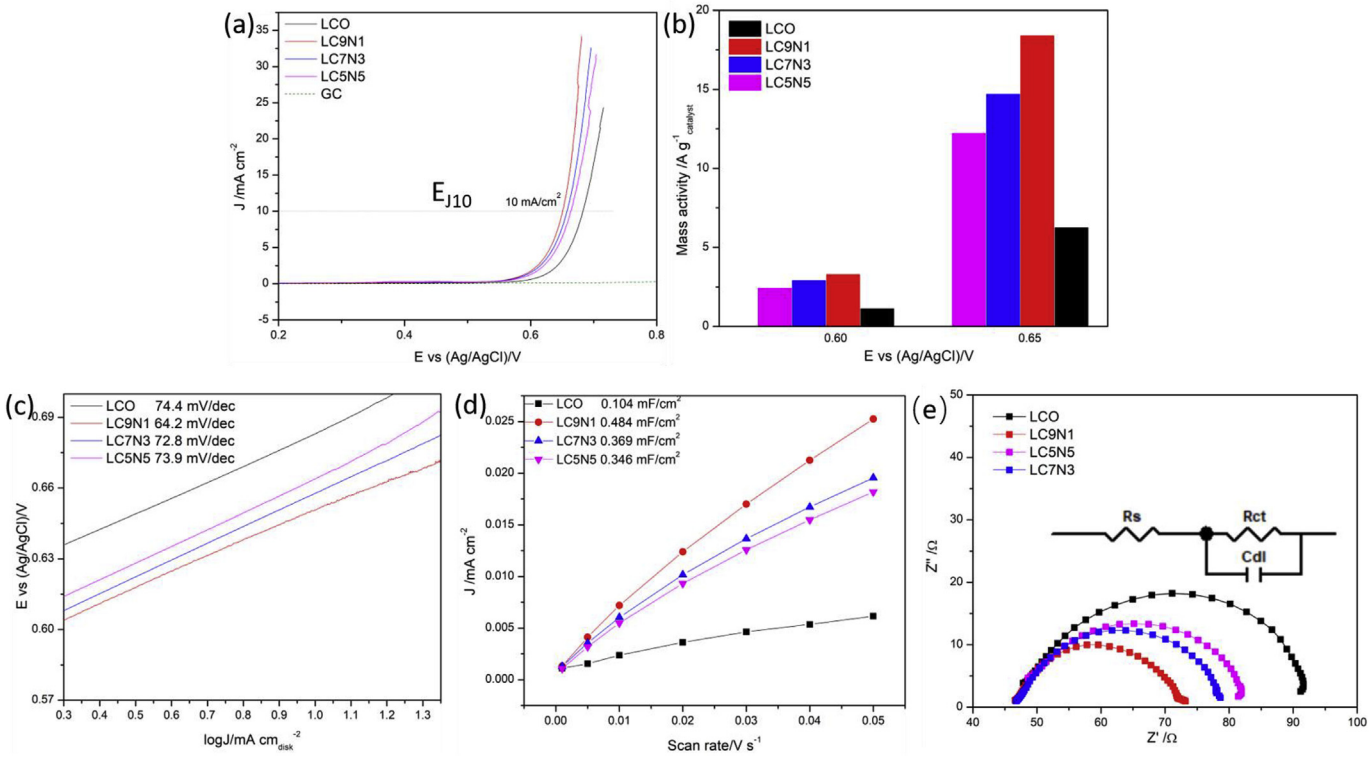

Fig. 5. LSV curves of OER at a rotation speed of 1600 rpm for four samples $LaCoO_3$, $LaCo_{0.9}Ni_{0.1}O_3$, $LaCo_{0.7}Ni_{0.3}O_3$ and $LaCo_{0.5}Ni_{0.5}O_3$ in 0.1 mol L^{-1} KOH solution with a scan rate of 10 mV/s; (b) Mass activity of the four samples at 0.6 V and 0.65 V vs Ag(s)|AgCl(s)|Cl^-(aq) (3.5 mol L^{-1} KCl); (c) Tafel plots of the four samples; (d) Double-layer capacitance measurements for determining electrochemically active surface area for $LaCo_{1-x}Ni_xO_3$ catalyst from cyclic voltammetry in 0.1 M KOH. The cathodic charging currents measured at 0.5 V vs Ag(s)|AgCl(s)|Cl^-(aq) (3.5 mol L^{-1} KCl) plotted as a function of scan rate. The determined double-layer capacitance of the system is taken as slope of the linear fits to the data; and (e) Nyquist plots of the four samples at 0.7 V vs Ag(s)|AgCl(s)|Cl^-(aq) (3.5 mol L^{-1} KCl) under an AC voltage of 5 mV. Inserted is the equivalent circuit.

Table 1
Comparison of the bifunctional catalytic activity for $LaCo_{1-x}Ni_xO_3$ (x = 0, 0.1, 0.3, 0.5) catalysts with noble-metal and some other reported perovskite-based catalysts. All the catalysts in the table were tested in 0.1 M KOH solution.

Catalyst	Scan rate	E_{ORR}@-1 mA cm^{-2}/V	E_{OER}@10 mA cm^{-2}/V	ΔE (V, E_{ORR}-E_{OER})	Reference
$LaCoO_3$	10 mV/s	−0.36 vs Ag/AgCl	0.68 vs Ag/AgCl	1.04	This work
$LaCo_{0.9}Ni_{0.1}O_3$	10 mV/s	−0.32 vs Ag/AgCl	0.65 vs Ag/AgCl	0.97	This work
$LaCo_{0.7}Ni_{0.3}O_3$	10 mV/s	−0.30 vs Ag/AgCl	0.657 vs Ag/AgCl	0.96	This work
$LaCo_{0.5}Ni_{0.5}O_3$	10 mV/s	−0.22 vs Ag/AgCl	0.66 vs Ag/AgCl	0.88	This work
Pt/C	10 mV/s	0.97 vs RHE	2.19 vs RHE	1.22	[42]
IrO_2	10 mV/s	0.38 vs RHE	1.70 vs RHE	1.32	[42]
$La_{0.95}FeO_3$	10 mV/s	0.58 vs RHE	1.64 vs RHE	1.06	[43]
$La_{0.5}Sr_{0.5}CoO_{2.91}$	5 mV/s	0.78 vs RHE	1.84 vs RHE	1.06	[44]
$BaMnO_3$	10 mV/s	−0.28 vs Ag/AgCl	0.90 vs Ag/AgCl	1.18	[10]
$La_{0.6}Sr_{0.4}CoO_{3-\delta}$	5 mV/s	−0.187 vs Hg/HgO	0.893 vs Hg/HgO	1.08	[13]
$BaTiO_3$	5 mV/s	0.72 vs RHE	1.90 vs RHE	1.18	[45]
$La_{0.8}Sr_{0.2}MnO_3$	10 mV/s	−0.13 vs Ag/AgCl	0.95 vs Ag/AgCl	1.08	[11]

simulation results, the charge transfer resistance Rct of $LaCo_{0.9}Ni_{0.1}O_3$ is 23.47 Ω, the smallest among these catalysts. $LaCoO_3$ exhibited a relatively larger Rct (41.88 Ω) than both $LaCo_{0.7}Ni_{0.3}O_3$ (26.68 Ω) and $LaCo_{0.5}Ni_{0.5}O_3$ (32.27 Ω). This result suggests that the $LaCo_{0.9}Ni_{0.1}O_3$ electrode possessed excellent charge transfer ability, which is consistent with the Nyquist plots and agrees well with the LSV results of OER, shown in Fig. 5a.

The bifunctionality of the catalysts for both ORR and OER could be examined using the potential difference between E_{J10} (the OER potential at current density of 10 mA/cm^2) and E_{J-1} (ORR potential at current density of −1 mA/cm^2) [11]. Smaller potential difference ΔE ($\Delta E = E_{J10}-E_{J-1}$) indicates much better electrocatalytic performance for both OER and ORR. This ΔE values can be calculated based on Fig. S6, which are found to be 1.04, 0.97, 0.96 and 0.88 V for $LaCoO_3$, $LaCo_{0.9}Ni_{0.1}O_3$, $LaCo_{0.7}Ni_{0.3}O_3$ and $LaCo_{0.5}Ni_{0.5}O_3$, respectively. The comparison of the bifunctional performance between the as-prepared catalysts and other reported catalysts has been listed in Table 1. The results indicate that $LaCo_{0.5}Ni_{0.5}O_3$ has the best bifunctionality among the as-prepared samples due to its high ORR performance, which is comparable to or even better than the state-of-the-art bifunctional catalysts as reported in the literature. Furthermore, the stability of $LaCo_{0.5}Ni_{0.5}O_3$ performance for both OER and ORR has been examined using cycling voltammetry scans between 0.2 and 1 V (versus Ag(s)|AgCl(s)|Cl^-(aq) (3.5 mol L^{-1} KCl)) at a scan rate of 50 mV/s in 0.1 M KOH for 1000 cycles. As shown in Fig. 6, it has been observed that LSV scan after 1000 cycles showed 20 mV positive shift for achieving a current density of 10 mA/cm^2 in OER and 24 mV negative shift for a current density of −1 mA/cm^2 for ORR, which confirmed the comparatively high durability of $LaCo_{0.5}Ni_{0.5}O_3$ perovskite oxide in 0.1 M KOH alkaline solution. The stability test (Fig. S7) for the other synthesized perovskite oxides $LaCoO_3$, $LaCo_{0.9}Ni_{0.1}O_3$ and $LaCo_{0.7}Ni_{0.3}O_3$ also have been examined, which further indicates the relatively good stability of the as-prepared perovskite oxides in alkaline solution, suggesting that the as-prepared perovskites might be good candidates as oxygen catalysts in fuel cell or metal-air batteries.

4. Conclusion

In summary, polymer-assisted method has been utilized to prepare $LaCoO_3$-based perovskite oxides with porous network structures which are composed of interconnected nanoparticles with size of 30–80 nm. The electrocatalytic performance of the as-prepared metal oxides for both ORR and OER in alkaline solutions has been examined, which shows that the bifunctionality of the catalysts could be enhanced via incorporation of Ni. The improvement of catalytic activity of $LaCo_{0.5}Ni_{0.5}O_3$ both in OER (33 mV negative shift for the E_{J10} potential compared with $LaCoO_3$) and

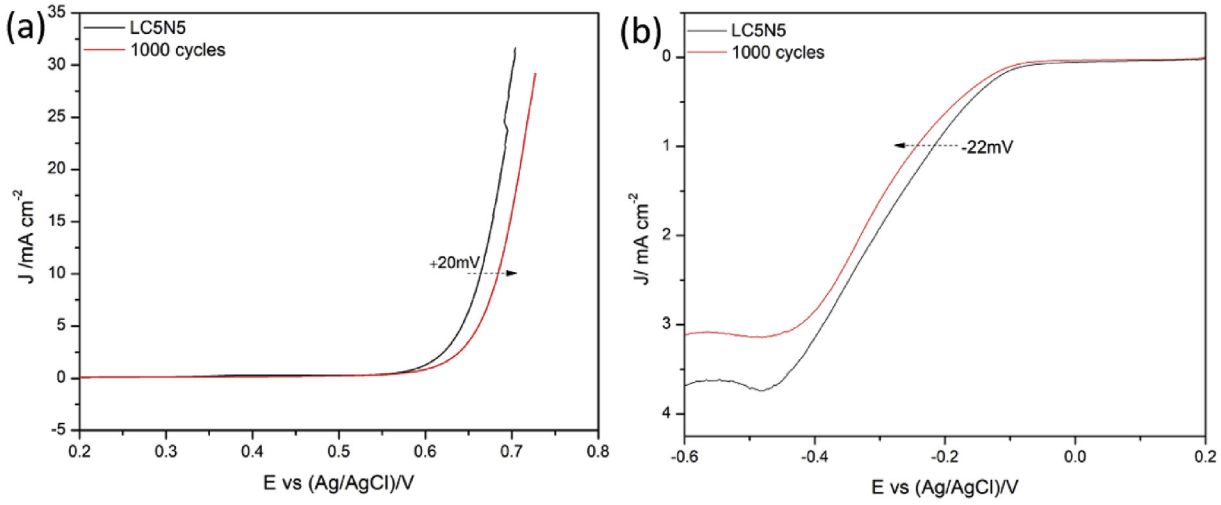

Fig. 6. Stability test of $LCo_{0.5}Ni_{0.5}O_3$. OER (a) and ORR (b) linear sweep voltammograms (LSVs) on rotating disk electrodes for $LCo_{0.5}Ni_{0.5}O_3$ before and after 1000 cycles testing in O_2-saturated 0.1 M KOH solution at a scan rate of 50 mV/s with a rotation speed of 1600 rpm.

ORR (145 mV positive shift for the E_{J-1} potential compared with $LaCoO_3$) could be observed. The improved electrocatalytic performance might be due to the synergistic effect from the two transition metal ions from the existence of mixed valence states of Co^{3+}/Co^{2+} and Ni^{3+}/Ni^{2+} with optimized composition and tunable OH-adsorption and O_2 desorption ability. The bifunctionality of the synthesized perovskite oxides as oxygen catalysts showed comparable or even better performance than the reported perovskite-based catalysts. The stability test of the as-prepared materials also indicates that Ni-doped $LaCoO_3$ might be good candidates as oxygen catalysts in fuel cells or metal-air batteries.

Acknowledgements

Dr. Luo thanks the support from New Mexico EPSCoR with NSF-1301346 and USDA National Institute of Food and Agriculture, HSI Collaboration: Integrating Food Science/Engineering and Education Network (IFSEEN, award number: 2015-38422-24059). Dr. Zhou thanks the support from Idaho National Laboratory (198992).

Appendix A. Supplementary data

Supplementary data to this article can be found online at https://doi.org/10.1016/j.electacta.2018.11.075.

References

[1] X.W. Yu, S.Y. Ye, Recent advances in activity and durability enhancement of Pt/C catalytic cathode in PEMFC-Part II: degradation mechanism and durability enhancement of carbon supported platinum catalyst, J. Power Sources 172 (2007) 145–154.
[2] M.J. Chen, L. Wang, H.P. Yang, S. Zhao, H. Xu, G. Wu, Nanocarbon/oxide composite catalysts for bifunctional oxygen reduction and evolution in reversible alkaline fuel cells: a mini review, J. Power Sources 375 (2017) 277–290.
[3] J. Xiao, D.H. Wang, W. Xu, D.Y. Wang, R.E. Williford, J. Liu, J.G. Zhang, Optimization of air electrode for Li/air batteries, J. Electrochem. Soc. 157 (2010) 487–492.
[4] S. Mao, Z.H. Wen, T.Z. Huang, Y. Hou, J.H. Chen, High-performance bi-functional electrocatalysts of 3D crumpled graphene-cobalt oxide nanohybrids for oxygen reduction and evolution reactions, Energy Environ. Sci. 7 (2014) 609–616.
[5] X.X. Wang, S. Hwang, Y.T. Pan, K. Chen, Y.H. He, S. Karakalos, H.G. Zhang, J.S. Spendelow, D. Su, G. Wu, Ordered Pt_3Co intermetallic nanoparticles derived from metal-organic frameworks for oxygen reduction, Nano Lett. 18 (2018) 4163–4171.
[6] R.G. Gonzalez-Huerta, J.A. Chavez-Carvayar, O. Solorza-Feria, Electrocatalysis of oxygen reduction on carbon supported Ru-based catalysts in a polymer electrolyte fuel cell, J. Power Sources 153 (2006) 11–17.
[7] J.C. Cruz, V. Baglio, S. Siracusano, R. Ornelas, L. Ortiz-Frade, L.G. Arriaga, V. Antonucci, A.S. Arico, Nanosized IrO_2 electrocatalysts for oxygen evolution reaction in an SPE electrolyzer, J. Nanopart. Res. 13 (2011) 1639–1646.
[8] W.C. Xu, L.T. Yan, L. Teich, S. Liaw, M. Zhou, H.M. Luo, Polymer-assisted chemical solution synthesis of $La_{0.8}Sr_{0.2}MnO_3$-based perovskite with A-site deficiency and cobalt-doping for bifunctional oxygen catalyst in alkaline media, Electrochim. Acta 273 (2018) 80–87.
[9] H. Liu, X.F. Ding, L.X. Wang, D. Ding, S.H. Zhang, Cation deficiency design: a simple and efficient strategy for promoting oxygen evolution reaction activity of perovskite electrocatalyst, Electrochim. Acta 259 (2018) 1004–1010.
[10] Y. Xu, A. Tsou, Y. Fu, J. Wang, J.H. Tian, R.Z. Yang, Carbon-coated perovskite $BaMnO_3$ porous nanorods with enhanced electrocatalytic properites for oxygen reduction and oxygen evolution, Electrochim. Acta 174 (2015) 551–556.
[11] L.T. Yan, Y. Lin, X. Yu, W.C. Xu, T. Salas, H. Smallidge, M. Zhou, H.M. Luo, $La_{0.8}Sr_{0.2}MnO_3$-Based perovskite nanoparticles with the A-site deficiency as high performance bifunctional oxygen catalyst in alkaline solution, ACS Appl. Mater. Interfaces 9 (2017) 23820–23827.
[12] H.Z. Wang, B. Patterson, J.Z. Yang, D. Huang, Y. Qin, H.M. Luo, Polymer-assisted deposition of $SrTiO_3$ film as cathode buffer layer in inverted polymer solar cells, Appl. Mater. Today 9 (2017) 402–406.
[13] M.Y. Oh, J.S. Jeon, J.J. Lee, P. Kim, K.S. Nahm, The bifunctional electrocatalytic activity of perovskite $La_{0.6}Sr_{0.4}CoO_{3-\delta}$ for oxygen reduction and evolution reactions, RSC Adv. 5 (2015) 19190–19198.
[14] C. Jin, X.C. Cao, F.L. Lu, Z.R. Yang, R.Z. Yang, Electrochemical study of $Ba_{0.5}Sr_{0.5}Co_{0.8}Fe_{0.2}O_3$ perovskite as bifunctional catalyst in alkaline media, Int. J. Hydrogen Energy 38 (2013) 10389–10393.
[15] A. Costa, M.E.M. Jorge, M.D. Carvalho, A. Gomes, M.I.S. Pereira, $LaNi_{1-x}Cu_xO_3$ (x =0.05, 0.10, 0.30) coated electrodes for oxygen evolution in alkaline medium, J. Sold State Electrochem. 17 (2013) 2311–2318.
[16] C. Jin, X.C. Cao, L.Y. Zhang, C. Zhang, R.Z. Yang, Preparation and electrochemical properties of urchin-like $La_{0.8}Sr_{0.2}MnO_3$ perovskite oxide as a bifunctional catalyst for oxygen reduction and oxygen evolution reaction, J. Power Sources 241 (2013) 225–230.
[17] H.Y. Zhu, P.F. Zhang, S. Dai, Recent advances of lanthanum-based perovskite oxides for catalysis, ACS Catal. 5 (2015) 6370–6385.
[18] D.B. Meadowcroft, Low-cost oxygen electrode material, Nature 226 (1970) 847–848.
[19] Z.Z. Du, P. Yang, L. Wang, Y.H. Lu, J.B. Goodenough, J. Zhang, D.W. Zhang, Electrocatalytic performances of $LaNi_{1-x}Mg_xO_3$ perovskite oxides as bifunctional catalysts for lithium air batteries, J. Power Sources 265 (2014) 91–96.
[20] F. Teng, S. Liang, B. Gaugeu, R. Zong, W. Yao, Y. Zhu, Carbon nanotubes-templated assembly of $LaCoO_3$ nanowires at low temperatures and its excellent catalytic properties for CO oxidation, Catal. Commun. 8 (2007) 1748–1754.
[21] J. Shim, K.J. Lopez, H.-J. Sun, G. Park, J.-C. An, S. Eom, S. Shimpalee, J.W. Weidner, Preparation and characterization of electrospun $LaCoO_3$ fibers for oxygen reduction and evolution in rechargeable Zn-air batteries, J. Appl. Electrochem. 45 (2015) 1005–1012.
[22] S.Y. Bie, Y.Q. Zhu, J.M. Su, C. Jin, S.H. Liu, R.Z. Yang, J. Wu, One-pot fabrication of yolk-shell structured $La_{0.9}Sr_{0.1}CoO_3$ perovskite microspheres with enhanced catalytic activities for oxygen reduction and evolution reactions, J. Mater. Chem. A 3 (2015) 22448–22453.
[23] C.Y. Zhu, A. Nobuta, I. Nakatsugawa, T. Akiyama, Solution Combustion synthesis of $LaMO_3$ (M= Fe, Co, Mn) perovskite nanoparticles and the measurement of their electrocatalytic properties for air cathode, Int. J. Hydrogen Energy 38 (2013) 13238–13248.
[24] N.P. Bansal, Z. Zhang, Combustion synthesis of $Sm_{0.5}Sr0_{.5}CoO_{3-x}$ and $La_{0.6}Sr_{0.4}CoO_{3-x}$ nanopowders for solid oxide fuel cell cathodes, J. Power Sources 158 (2006) 148–153.
[25] S. Nakayama, $LaFeO_3$ perovskite-type oxide prepared by oxide-mixing, co-precipitation and complex synthesis methods, J. Mater. Sci. 36 (2001) 5643–5648.
[26] M.E. Baydi, S.K. Tiwari, R.N. Singh, J.L. Rehspringer, P. Chartier, J.F. Koenig, G. Poillerat, High specific surface area nickel mixed oxide powders $LaNiO_3$ (perovskite) and $NiCo_2O_4$ (spinel) via sol-gel type routes for oxygen electrocatalysis in alkaline media, J. Solid State Chem. 116 (1995) 157–169.
[27] H. Kozuka, K. Ohbayashi, K. Koumoto, $LaCo_{1-x}Ni_xO_3$ with improved electrical conductivity, Inorg. Chem. 51 (2012) 9259–9264.
[28] V. Kumar, R. Kumar, D.K. Shukla, S. Gautam, K.H. Chae, Electronic structure and electrical transport properties of $LaCo_{1-x}Ni_xO_3$ (0<x<0.5), J. Appl. Phys. 114 (2013), 073704.
[29] V. Vulchev, L. Vassilev, S. Harizanova, M. Khristov, E. Zhecheva, R. Stoyanova, Improving of the thermoelectric efficiency of LaCoO3 by double substitution with nickel and iron, J. Phys. Chem. C 116 (2012) 13507–13515.
[30] S. Ivanova, A. Senyshyn, E. Zhecheva, K. Tenchev, R. Stoyanova, H. Fuess, Crystal structure, microstructure and reducibility of $LaNi_xCo_{1-x}O_3$ and $LaFe_xCo_{1-x}O_3$ Perovskites (0<x<0.5), J. Solid State Chem. 183 (2010) 940–950.
[31] R. Robert, L. Bocher, B. Sipos, M. Dobeli, A. Weidenkaff, Ni-doped cobaltates as potential materials for high temperature solar thermoelectric converters, Prog. Solid State Chem. 35 (2007) 447–455.
[32] Q.H. Qi, P.F. Zhai, Y.H. Sun, J. Zhao, B.Q. Sun, B. Patterson, H.M. Luo, W.R. Zhang, L. Jiao, H.Y. Wang, G.F. Zou, Aqueous solution-deposited molybdenum oxide films as an anode interfacial layer for organic solar cells, ACS Appl. Mater. Interfaces 7 (2015) 18218–18224.
[33] Q.X. Jia, T.M. McCleskey, A.K. Burrell, Y. Lin, G.E. Collis, H. Wang, A.D.Q. Li, S.R. Foltyn, Polymer-assisted deposition of metal-oxide films, Nat. Mater. 3 (2004) 529–532.
[34] G.F. Zou, J. Zhao, H.M. Luo, T.M. McCleskey, A.K. Burrell, Q.X. Jia, Polymer-assisted-deposition: a chemical solution route for a wide range of materials, Chem. Soc. Rev. 42 (2013) 439–449.
[35] H. Osgood, S.V. Devaguptapu, H. Xu, J. Cho, G. Wu, Transition metal (Fe, Co, Ni and Mn) oxides for oxygen reduction and evolution bifunctional catalysts in alkaline media, Nano Today 111 (2016) 601–625.
[36] A. Vignesh, M. Prabu, S. Shanmugam, Porous $LaCo_{1-x}Ni_xO_{3-\delta}$ nanostructures as an efficient electrocatalyst for water oxidation and for a zinc-air battery, ACS Appl. Mater. Interfaces 8 (2016) 6019–6031.
[37] P. Xiao, J.J. Zhu, H.L. Li, W. Jiang, T. Wang, Y.J. Zhu, Y.X. Zhao, J.J. Li, Effect of textural structure on the catalytic performance of $LaCoO_3$ for CO oxidation, ChemCatChem 6 (2014) 1774–1781.
[38] Y.X. Wang, X.Z. Cui, Y.S. Li, L.S. Chen, Z. Shu, H.R. Chen, J.L. Sshi, High surface area mesoporous $LaFe_xCo_{1-x}O_3$ oxides: synthesis and electrocatalytic property for oxygen reduction, Dalton Trans. 42 (2013) 9448–9452.
[39] L. Qiao, X.F. Bi, Direct observation of Ni^{3+} and Ni^{2+} in correlated $LaNiO_{3-\delta}$ films, Europhys. Lett. 93 (2011) 57002 (p57001-p57006).
[40] M. Risch, Perovskite electrocatalysts for the oxygen reduction reaction in alkaline media, Catalysts 7 (2017) 154–184.
[41] T. Otagawa, J.O.M. Bockris, The electrocatalysis of oxygen evolution on perovskites, J. Electrochem. Soc. 131 (1984) 290–302.
[42] R.A. Rincon, J. Masa, S. Mehrpour, F. Tietz, W. Schuhmann, Activation of oxygen evolving perovskites for oxygen reduction by functionalization with Fe-Nx/C groups, Chem. Commun. 50 (2014) 14760–14762.
[43] Y.L. Zhu, W. Zhou, J. Yu, Y.B. Chen, M.L. Liu, Z.P. Shao, Enhancing

electrocatalytic activity of perovskite oxides by tuning cation deficiency for oxygen reduction and evolution reactions, Chem. Mater. 28 (2016) 1691–1697.
[44] Y. Zhao, L. Xu, L. Mai, C. Han, Q. An, X. Liu, Q. Zhang, Hierarchical mesoporous perovskite $La_{0.5}Sr_{0.5}CoO_{2.91}$ nanowires with ultrahigh capacity for Li-air batteries, Proc. Natl. Acad. Sci. 109 (2012) 19569–19574.
[45] C.F. Chen, G. King, R.M. Dickerson, P.A. Papin, S. Gupta, W.R. Kellogg, G. Wu, Oxygen-deficient $BaTiO_3$ perovskite as an efficient bifunctional oxygen electrocatalyst, Nano Energy 13 (2015) 423–432.